Journal of The Electrochemical Society

Investigating the Influence of Cr and Mo Additions to Commercial Ni-Based Alloys Exposed to Neutral and Acidic Chloride Solutions

Journal of The Electrochemical Society, 2020 **167** 131512

Investigating the Influence of Cr and Mo Additions to Commercial Ni-Based Alloys Exposed to Neutral and Acidic Chloride Solutions

Jeffrey D. Henderson,[1,*,z] Baian Almusned,[1,*] Mojtaba Momeni,[1] Samantha Anderson,[1] Vahid Dehnavi,[2] Dmitrij Zagidulin,[1,] David W. Shoesmith,[1,2,***] and James J. Noël [1,2,**]**

[1]*Department of Chemistry, Western University, London, ON N6A 5B7, Canada*
[2]*Surface Science Western, Western University, London, ON N6G 0J3, Canada*

The corrosion behaviour of four commercially available Ni-based alloys is presented for both natural and potential-controlled corrosion in chloride solutions. Electrochemical evidence suggests a balance of Cr and Mo is essential to maintaining passive film stability in chloride solutions, especially those in which acidic conditions may develop. In near-neutral solutions, increased Cr content results in lower corrosion rates and improved passive properties; however, an increase in Cr content above 15 wt.% provided only minor additional benefits. In acidic solutions, Mo content is essential to corrosion resistance and imparts two major benefits: increased film stability and rapid repassivation of breakdown events. Since localized corrosion and the critical chemistry which accompanies these processes are of concern in many chloride-containing applications, a delicate balance of Cr and Mo must be considered; although optimal concentrations have yet to be determined.

 [DOI: 10.1149/1945-7111/abbea7]

Manuscript submitted August 6, 2020; revised manuscript received September 29, 2020. Published October 14, 2020.

Supplementary material for this article is available online

Corrosion-resistant alloys, such as those based on a Ni-matrix, rely on additions of Cr and Mo, among other alloying elements (e.g., W, Cu, etc.), to promote the formation of an oxide film. Serving as a physical barrier, the oxide functions by slowing the dissolution of the underlying reactive substrate.[1] With applications of these alloys in the nuclear, aerospace, chemical, and petrochemical processing industries, a thorough understanding of the passive film, in relation to alloy composition, is essential for both proper material selection and accurate lifetime assessments. In neutral solutions (pH $\sim$ 7), oxides formed on Cr-containing alloys have been shown to be dominated by a Cr^{III}-rich barrier layer and as a result, exhibit excellent corrosion resistance.[2,3] However, in acidic environments, the increased solubility of Cr^{III} species can lead to the destruction of this passive layer.[4,5] Additions of Mo have been shown to increase the resistance to corrosion in acidic solutions. Empirical relationships such as the pitting resistance equivalent number (PREN)[6] and the atomic percent factor (APF)[7,8] have been successfully used to describe the benefits Cr and Mo; but are limited in the mechanistic information they provide. While the relationship between alloyed Cr and Mo has been extensively studied,[9–11] ongoing research[3,12–16] continues to provide new information.

High chloride solutions are of principal interest, due to their industrial relevance and their importance in the mechanism of crevice corrosion.[17] Crevice corrosion has been regarded as a potentially dangerous process for Ni–Cr–Mo alloys, due to its difficult detection, unpredictability, and self-sustaining nature. While Ni–Cr–Mo alloys are considered immune to pitting in near-neutral chloride environments, the presence of an occluded geometry can lead to local acidification which may eventually challenge the integrity of the passive film. According to some studies, the pH inside an active crevice on Ni–Cr–Mo alloys can be as low as zero.[10,18] Once activated, metal dissolution inside the crevice couples to O_2 reduction on surfaces outside the crevice, and with H^+ reduction inside the crevice.[19] Previously,[20] we have shown that the contribution of H^+ reduction can almost double the extent of corrosion damage, but decreases as the Mo content of the alloy increases. Due to the potential severity of crevice corrosion, it is essential to understand the relationship between alloyed Cr and Mo and the corrosion reaction in conditions anticipated both inside and outside a crevice; i.e., in acidic and near-neutral chloride solutions, respectively. Through an improved understanding, alloy compositions, as well as lifetime assessments, may be optimized.

The corrosion behaviour of four commercially available Ni-based alloys, Hastelloy BC-1, C-22, G-35, and G-30, has been investigated in 3 M NaCl and 1 M HCl + 2 M NaCl solutions at 75 °C. While acidity is of primary interest, the importance of cathodic reactions (O_2 and H^+ reduction) was also investigated by changing the O_2 concentration. Furthermore, both the open-circuit and polarization behaviours were investigated. Here, discussion is limited to electrochemical studies, including corrosion potential (E_{CORR}) monitoring, linear polarization resistance (LPR), electrochemical impedance spectroscopy (EIS), and both dynamic and static polarization measurements. A complementary study of film composition is underway.

Experimental

Sample preparation.—Materials were provided by Haynes International (Kokomo, IN, USA) in the mill-annealed sheet form. Nominal compositions, as reported by the manufacturer, are summarized in Table I, while the measured compositions, determined by inductively coupled plasma atomic emission spectroscopy (ICP-AES, Cambridge Materials Testing Limited, Cambridge, ON), are summarized in Table II. Unless otherwise stated, discussions will refer to the nominal composition provided by the manufacturer.

Experimental coupons were fabricated with the dimensions 0.6 × 0.6 × 6 cm^3. Avoiding the use of epoxy and the subsequent opportunity for crevice corrosion to occur, these "stick" electrodes were partially submerged directly in the experimental solutions. Observations of minimal waterline corrosion were made only in naturally aerated acidic solutions and were considered insignificant compared to corrosion damage present elsewhere on the coupon. Prior to all measurements, coupons were ground to a final surface preparation of P1200 using wet SiC paper with water as lubricant. Coupons were then sonicated in ethanol (95%), rinsed in type-1 water (18.2 MΩ cm), and dried in a stream of ultra-high purity Ar gas (Praxair, Mississauga, ON). Applying this procedure ensured that the surfaces demonstrated reproducible electrochemical behaviour.

Solutions were prepared using reagent grade NaCl and concentrated HCl (Caledon Laboratory Chemicals, Georgetown, ON). The

*Electrochemical Society Student Member.
**Electrochemical Society Member.
***Electrochemical Society Fellow.
[z]E-mail: jhende64@uwo.ca

Table I. Nominal compositions of the examined alloys (wt.%) as reported by Haynes International. Maximum allowable concentrations are indicated by "M". The balance of the composition is nickel in each of these alloys.

Alloy	Ni	Cr	Mo	Fe	W	Cu	Nb	Co	Mn	V	Al	Si	C
G-35	Bal.	33.2	8.1	2^{M}	0.6	0.3^{M}	—	1^{M}	0.5^{M}	—	0.4^{M}	0.6^{M}	0.05^{M}
G-30	Bal.	30	5.5	15	2.5	2	0.8	5	1.5	—	—	0.8^{M}	0.03^{M}
C-22	Bal.	22	13	3	3	0.5^{M}	—	2.5^{M}	0.5^{M}	0.35^{M}	—	0.08^{M}	0.01^{M}
BC-1	Bal.	15	22	2^{M}	—	—	—	—	0.25	—	0.5^{M}	0.08^{M}	0.01^{M}

chloride concentration in all solutions was kept constant by substituting NaCl for HCl in equimolar quantities, with the studied concentrations being 3 M NaCl and 1 M HCl + 2 M NaCl. Where indicated, dissolved O_2 was removed by an initial high rate of sparging with ultra-high purity Ar followed by continuous sparging for the duration of the experiment.

Electrochemical methods.—Experiments were conducted in a three-compartment glass electrochemical cell. A water jacket, which encased the main compartment, was connected to an isothermal water circulator. The circulator was used to maintain a solution temperature of 75 ± 1 °C. The counter electrode (CE), a platinum flag, and the reference electrode (RE), a saturated calomel electrode (SCE), were housed in their own compartments, isolated from the main compartment by porous glass frits. Prior to each experiment, the RE was calibrated against a "master" electrode, used only for calibration purposes. Following each experiment, the surface area of the "stick" working electrode (WE) was measured to allow for the conversion of the measured current into current density.

Electrochemical measurements were made using either a Model 1287 potentiostat or 2100 Analytical Modulab (Solartron Analytical, Hampshire, UK). Corrosion behaviour was studied by monitoring the corrosion potential (E_{CORR}) for a period of 6 h, with linear polarization resistance (LPR) measurements made every 30 min. LPR measurements involved polarizing the WE ± 10 mV (vs E_{CORR}) at a scan rate of 10 mV min^{-1}. Polarization resistance (R_P) values were then calculated from the slopes of the linear current density (j) vs potential (E) plots (i.e., $R_P = \Delta E/\Delta j$). In separate experiments, electrochemical impedance spectroscopy (EIS) measurements were performed at the end of a 6-h E_{CORR} measurement. Spectra were acquired at E_{CORR} by the application of a sinusoidal perturbation (± 10 mV) at 11 points per decade in the frequency range from 10^5 to 10^{-3} Hz. A second spectrum was recorded using a frequency scan in the reverse direction to ensure that the system under investigation was stable during the EIS measurement.

In the study of polarization behaviour, both dynamic- and static-polarization techniques were used. Dynamic experiments were initiated at −0.050 V (vs E_{CORR}) and scanned in the positive direction at 10 mV min^{-1} until either the potential reached 1.1 V (vs SCE) or the absolute current reached 10 mA. In static experiments, a fixed potential of 0 V (vs SCE), was applied and the resulting current response monitored as a function of time.

Results

Corrosion potential (E_{CORR}) and polarization (R_p) measurements.—During immersion in near-neutral chloride solution, all alloys exhibited behaviour consistent with the formation of a passive film. A summary of E_{CORR} and R_P measurements made in aerated 3 M NaCl is given in Fig. 1A. Overall, both E_{CORR} and R_P were found to increase toward steady-state values. For all alloys, R_P values were found to be on the order of 10^6 Ω.cm^2, consistent with the passive behaviour expected for these alloys in nonaggressive solutions,[2,21] and with the rapid formation of a Cr-rich oxide barrier layer.[22,23] Values of R_P increased only slightly with the Cr content of the alloy: BC-1 (15 wt.% Cr) <C-22 (22 wt.% Cr) <G-30 (30 wt.% Cr) <G-35 (33.2 wt.% Cr). The benefit of increasing the Cr content >15 wt.% was minor.

Unlike R_P values, E_{CORR} exhibited no clear dependence on the Cr content of individual alloys. Previously, Lloyd et al. showed that an increased Cr content led to open-circuit ennoblement.[22] In the present work, this was found to be true only for BC-1, C-22 and G-30, whose E_{CORR} increased with Cr content: BC-1 (15 wt.% Cr) <C-22 (22 wt.% Cr) <G-30 (30 wt.% Cr). However, the highest-Cr-containing alloy, G-35 (33.2 wt.%), had the lowest E_{CORR} at the end of the 6-h immersion period. Based on the empirically determined alloy compositions, Table II, the E_{CORR} increased with Fe content in the order G-35 (0.54 wt.% Fe) ≈ BC-1 (0.85 wt.% Fe) <C-22 (3.74 wt.% Fe) <G-30 (14.75 wt.% Fe). This could be due to the presence of Fe_2O_3 or a Fe-containing spinel.[5,24] Since E_{CORR} is dependent on the kinetics of the anodic and cathodic half-reactions, this trend could indicate either increased anodic or decreased cathodic reaction kinetics.

A decrease in solution pH resulted in large changes to both E_{CORR} and R_P, compared to the values measured in near-neutral solution. The E_{CORR} and R_P values recorded in aerated 1 M HCl + 2 M NaCl solution are shown in Fig. 1B. Alloys C-22, G-30, and G-35, displayed comparable behaviour. Rather than increasing toward a steady-state, E_{CORR} rapidly stabilized and remained constant for the remainder of the experiment. It is worth mentioning that E_{CORR} values stabilized significantly faster in acidic solution than in the near-neutral chloride solution. This suggests that the rate of reaction in acidic solution is faster than that in near-neutral solution. Similarly, R_P quickly stabilized at low values, on the order of 10 Ω.cm^2. In this solution, R_P values were approximately five orders of magnitude lower than those measured in the near-neutral solution, indicating the establishment of active conditions. In acidic solution, the high solubility of Cr^{III} would be expected to challenge the Cr^{III} barrier layer.[25] Evidence for active conditions is presented below in the discussion of the dynamic polarization measurements.

Measurements on alloy BC-1 suggested the surface remained partially protected in acidic solution, Fig. 1B. Values of E_{CORR} rapidly increased to a maximum, which then decreased slightly with time. The maximum value was ~0.2 V higher than that measured in near-neutral solution. The negative-going transients observed in E_{CORR} suggest localized events occurring on the surface. Each

Table II. Actual compositions of the examined alloys (wt.%) as determined by ICP-AES. Chemical analysis was performed in accordance with ASTM E1019–18, E1097–12, and E1479–16.

Alloy	Ni	Cr	Mo	Fe	W	Cu	Mn	Al	Si	C
G-35	56.3	33.4	7.98	0.54	0.07	0.02	0.45	0.24	<0.01	<0.010
G-30	42.1	29.0	4.97	14.75	2.77	1.70	1.13	0.15	0.24	0.016
C-22	57.6	20.7	12.97	3.74	2.80	0.06	0.27	0.28	<0.01	0.012
BC-1	60.9	14.40	22.1	0.85	0.01	0.03	0.25	0.18	<0.01	0.011

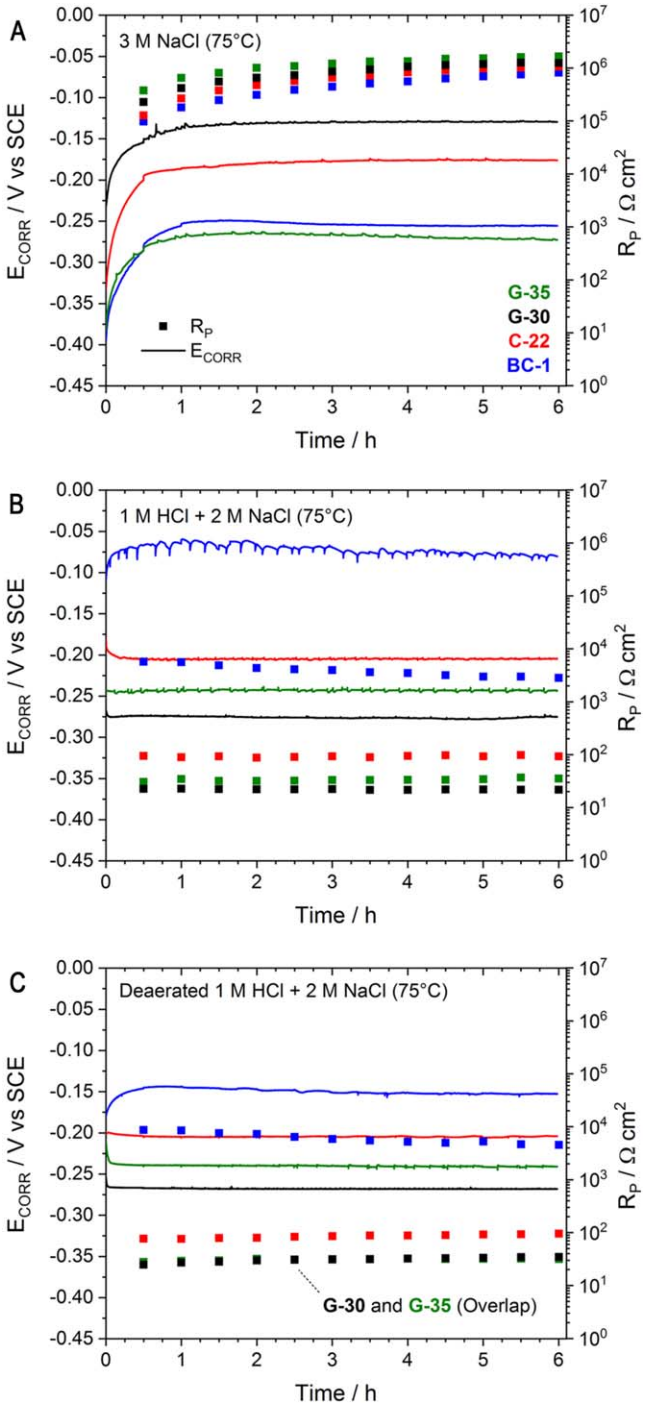

Figure 1. Corrosion potential (E_{CORR}) and polarization resistance (R_P) measurements on alloys BC-1, C-22, G-35, and G-30 exposed to (A) aerated 3 M NaCl, (B) aerated 1 M HCl + 2 M NaCl, and (C) deaerated 1 M HCl + 2 M NaCl (75 °C).

potential transient indicates a momentary acceleration of the anodic reaction, consistent with metastable pitting behaviour through a protective layer.[19,20] Unfortunately, the temporary influence of metastable events could not be captured by periodic R_P measurements. Values of R_P were on the order of 10^3 Ω.cm^2. While lower than those measured in near-neutral solution, they were approximately three orders of magnitude greater than values measured on alloys C-22, G-35, and G-30, exposed to the same solution. Together, these potential transients and the R_P values suggest that BC-1 maintains, at least to some extent, a partially protective passive film in an aerated 1 M HCl + 2 M NaCl solution. This combination of an increase in E_{CORR} and higher R_P values for BC-1 than on C-22, G-30, and G-35 alloys, suggests the anodic reaction is suppressed by the presence of a surface film. Given the high Mo content of BC-1, it is likely that this film is Mo-rich. It has been suggested that alloying with Mo stabilizes the Cr-rich oxide film in acidic solutions.[9,26–28] For Cr/Mo containing alloys, this is often attributed to the formation of a Mo-rich oxide layer over an inner Cr-rich barrier layer.[3,29–33] These results confirm a role for Mo in protecting an alloy from degenerating to active corrosion, providing the Mo content is >13 wt.%. For Mo <13 wt.%, any Cr^{III} barrier layer is dissolved and active corrosion can be achieved.

In addition to changes in behaviour caused by decreases in pH, changes caused by the removal of dissolved O_2 were also studied. The E_{CORR} and R_P values recorded in Ar-sparged 1 M HCl + 2 M NaCl are shown in Fig. 1C. For C-22, G-35, and G-30, the removal of O_2 produced E_{CORR} and R_P values comparable to those recorded in the naturally aerated acidic solution. This suggests that O_2 plays a minor role as the oxidant in comparison to H^+ at E_{CORR} when the alloy is active. In both aerated and deaerated solutions, E_{CORR} values for these alloys were near or below the equilibrium potential for H^+ reduction, −0.244 V (vs SCE) at pH 0 and 75 °C. In addition, the formation of bubbles was observed for alloys C-22 and G-35 and most copiously for alloy G-30. A comparison showing the formation of bubbles on alloy BC-1 and G-30 is included in the supporting information.

By contrast, the removal of dissolved O_2 caused noticeable changes in the behaviour of BC-1. The general trends in E_{CORR} were similar for both the aerated and the Ar-sparged solution conditions, i.e., a rapid increase followed by a gradual decline over the 6-h period. However, values measured in the Ar-sparged solution were found to be ∼0.1 V lower than those measured in naturally aerated solution. Additionally, the negative-going potential transients observed in the naturally aerated solution were absent in the Ar-sparged solution, confirming the role of O_2 in their generation. Previously, Ebrahimi et al. demonstrated that, while H^+ reduction was enough to maintain localized events on alloy BC-1, O_2 was an important oxidant during their initiation.[19] R_P values measured in Ar-sparged solution were only slightly higher than those measured in aerated solution.

Electrochemical impedance spectroscopy (EIS) measurements.—Representative impedance spectra collected in aerated 3 M NaCl solution are shown in Fig. 2. In Nyquist plots, not shown, depressed semi-circles with diameters on the order of 10^6 Ω.cm^2 were found for all alloys. This is consistent with the R_P values discussed above. The corresponding Bode plots are shown in Figs. 2A and 2B. The low frequency impedance modulus, |Z|, suggests that an increase in Cr-content provides only a minor benefit for Cr concentrations >15 wt.%. The phase angle plot shows two time-constants for all four alloys, one at high (∼10^3 Hz) and the other at low (∼10^{-1} Hz) frequency. The electrical equivalent circuit used to fit the spectra is shown in the inset of Fig. 2B. The impedance response of similar systems has been investigated and appropriate equivalent circuits discussed.[2,34–37] Ebrahimi et al. attributed the high and low frequency time-constants to interfacial charge transfer and film processes, respectively.[35] More complex circuits involving additional time-constants[2] have been proposed, including the need for diffusional (Warburg) elements to improve the fit of the equivalent circuit.[34,38] However, the inclusion of a Warburg element was not found to significantly improve the fit to the spectra in Fig. 2 and was therefore avoided.

In all cases, a constant phase element (CPE) was used in place of a capacitor to account for the non-ideal capacitive response of the surface.[39,40] For the low frequency time-constant, attributed to the response of the film, the CPE exponent was >0.85 for all alloys. On the other hand, CPE exponents corresponding to the interfacial process (∼10^3 Hz) were lower, suggesting the contribution of a diffusive impedance. Using the method developed by Brug et al.[41], the

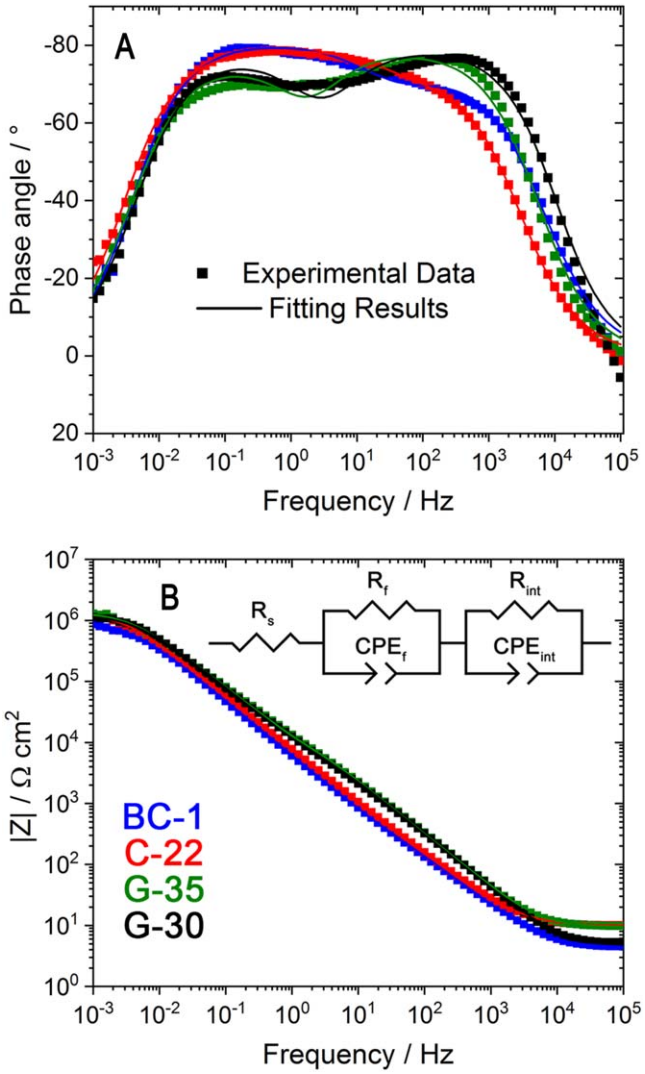

Figure 2. EIS recorded on alloys BC-1, C-22, G-35, and G-30 after 6 h exposure to aerated 3 M NaCl (75 °C). Points indicate experimental data while solid curves represent the result of equivalent circuit fitting.

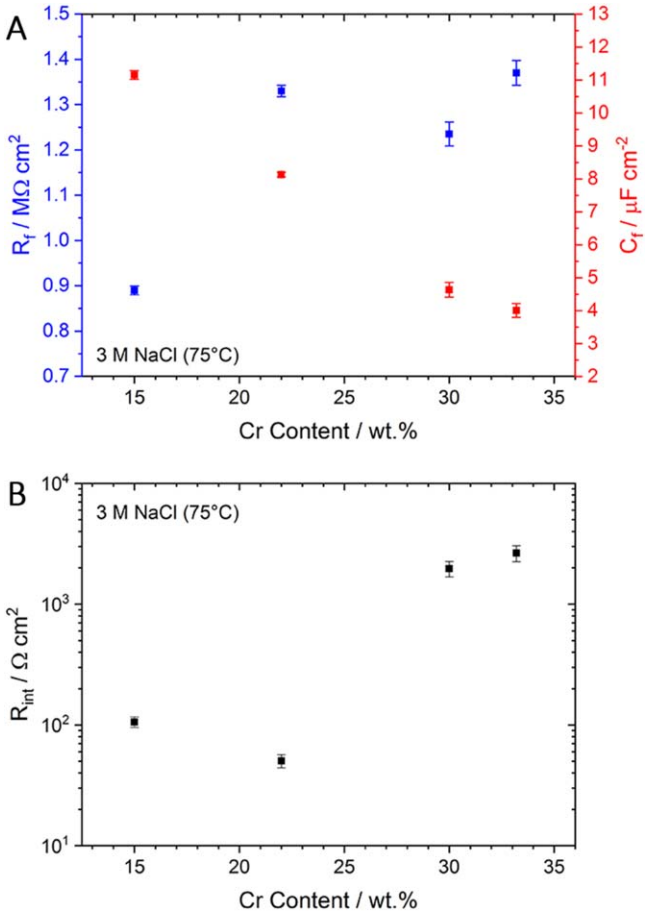

Figure 3. Dependence of (A) film resistance (R_f), film capacitance (C_f), and (B) interfacial resistance (R_{int}) on alloy Cr content after 6 h exposure to 3 M NaCl solution (75 °C). Values of capacitance were obtained from CPE_f according to the procedure proposed by Brug et al.[38]. The error bars indicate the goodness of fit obtained from linear least squares fitting.

CPE_f values were converted into equivalent capacitances (C_f) and plotted together with the resistance values (R_f). The results are plotted as a function of Cr content in Fig. 3A. In general, values of R_f increased with increasing Cr-content, except on G-30, for which R_f was lower than expected. This probably indicates an effect of the higher Fe content in G-30 on the passive film. Opposite to the trend in R_f, values of C_f were found to decrease with increasing Cr-content. The low values of C_f are in the range expected for a thin passive oxide. The increase in R_f, accompanied by a decrease in C_f, is consistent with an improvement in passive film properties due to its thickening and/or the elimination of point defects, with the latter reflected in a decrease in the dielectric constant of the film.[34,38] Overall, the impedance data presented here suggest that increasing Cr content to >15 wt.% results in only minor improvements in passivity. However, as is clear by inspection of Figs. 2A and 2B, significant differences in the alloy/oxide interfacial properties are observed. The interfacial resistance (R_{int}) for the two high Mo(W)/low Cr alloys, BC-1 and C-22, are considerably lower (by more than a factor of 10) than those for the high Cr/low Mo(W) alloys, Fig. 3B, with the low CPE exponents suggesting either a possible diffusive contribution or local film inhomogeneities. These results indicate a degradation of the inner barrier layer as the Mo(W)/Cr ratio is increased.

Representative impedance spectra collected in aerated 1 M HCl + 2 M NaCl are shown in Fig. 4. For alloy BC-1, two time-constants were observed, similar to the spectrum recorded in near-neutral 3 M NaCl, however, the absolute impedance was over two orders of magnitude lower. For the other alloys, the low frequency value of |Z| decreased to very low values, Fig. 4B. In addition, a low frequency inductive response, reflected in the temporary positive value of the phase angle, Fig. 4A, is observed. Such an inductive response may occur at sufficiently low frequencies for the BC-1 alloy but could not be detected in our experiments, since valid impedance data could only be recorded for frequencies $\geqslant 10^{-2}$ Hz. At lower frequencies, the film breakdown events observed in E_{CORR} measurements, Fig. 1B, led to erratic data. As a result, the impedance spectra violated the stability criterion required for valid data. Consequently, the circuit containing two RC time-constants, Fig. 4B (inset), was used to fit the spectra for BC-1, while the three time-constant circuit incorporating the inductor (L) and resistor (R_L), was used to fit the spectra recorded for the other three alloys.

Representative impedance spectra collected in deaerated 1 M HCl + 2 M NaCl are shown in Fig. 5. Values of |Z| were comparable with those observed in the aerated case and exhibited a similar overall increase as the Mo(W) content increased. As observed for aerated conditions, the spectrum obtained for BC-1 was fitted using the two time-constant circuit (inset to Fig. 5B). For the alloys undergoing active corrosion, the three time-constant circuit including L and R_L was required. Small changes in R_f, R_{int} and R_L were observed with no clear dependence on the Mo(W) content.

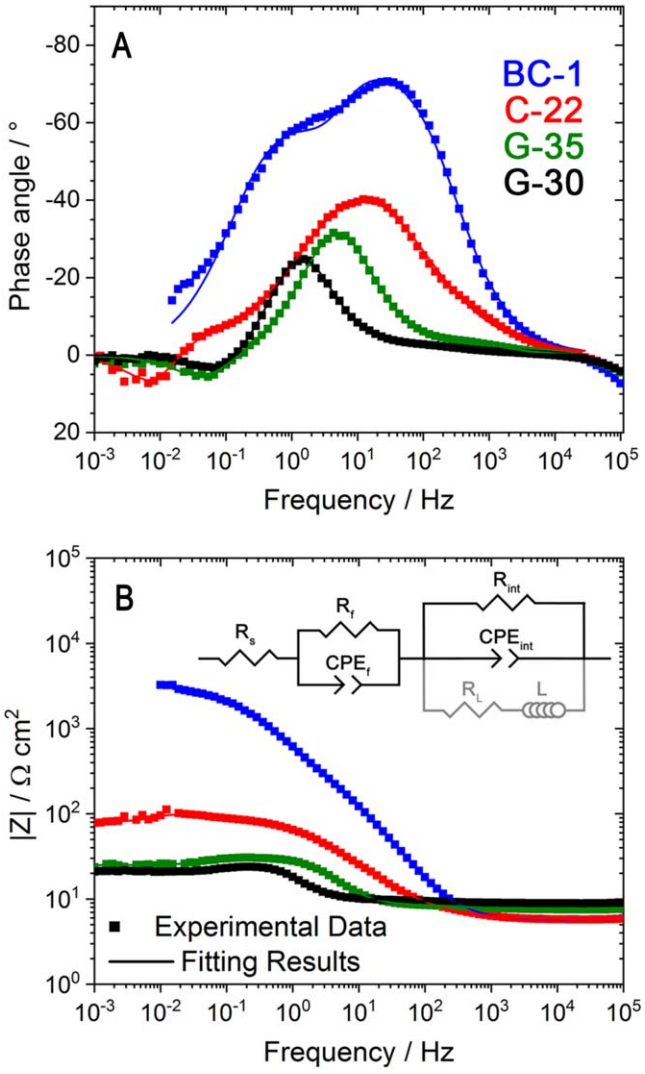

Figure 4. EIS recorded on alloys BC-1, C-22, G-35, and G-30 after 6 h exposure to aerated 1 M HCl + 2 M NaCl (75 °C). Points indicate experimental data while solid curves represent the result of equivalent circuit fitting.

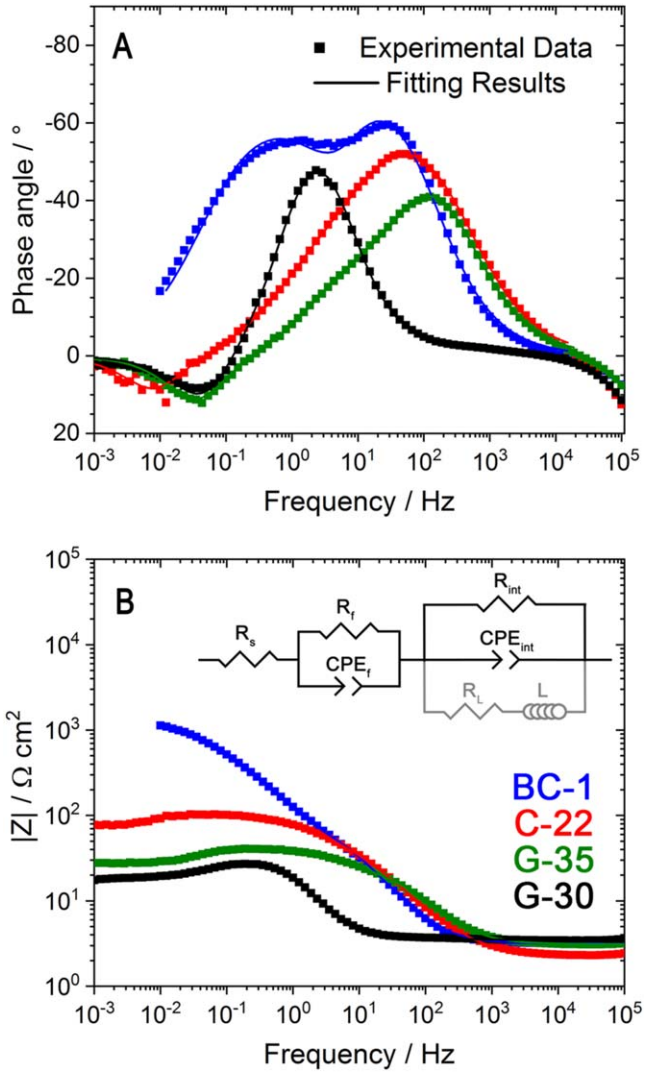

Figure 5. EIS recorded on alloys BC-1, C-22, G-35, and G-30 after 6 h exposure to deaerated 1 M HCl + 2 M NaCl (75 °C). Points indicate experimental data while solid curves represent the result of equivalent circuit fitting.

The overall influence of Mo and aeration on the resistive properties of the surface films is shown in Fig. 6, which plots the total interfacial resistance ($\Sigma R = R_f + R_{int} + R_L$) as a function of Mo content for both aerated and deaerated conditions, with the influence of aeration detectable only at the highest Mo content. Values of ΣR shown in Fig. 6 are comparable to R_P values discussed with Figs. 1B and 1C. Since the CPE exponents were in many cases <0.8, the conversion of the respective CPE parameters to capacitances was dubious. Of particular interest is the value for BC-1, since the impedance spectra show the presence of a substantial film while exposed to acidic solutions. Since the CPE exponent was >0.8 for aerated conditions the CPE was converted to an equivalent capacitance, yielding a value of 120 μF.cm^2, which is considerably higher than observed for neutral conditions, 11 μF.cm^2. Coupled with the relatively high value of R_f, this indicates the presence of a highly defective surface film. Similarly, high values of capacitance are observed under transpassive conditions[34] when the destruction of the Cr^{III} barrier layer at high potentials leads to the formation of a partially protective Mo-dominated layer.

Dynamic and static polarization measurements.—Figure 7A shows linear polarization curves recorded in a neutral 3 M NaCl solution. For potentials positive of E_{CORR}, all the alloys exhibited a passive region, extending up to ~0.2 V (vs SCE). For the three high-Cr alloys, the current densities in the passive region were effectively the same, while that for the BC-1 alloy was noticeably higher, as expected, given its lower Cr content. For higher potentials, the film thickness has been shown to increase,[32] however, the onset of Cr^{III} oxidation to Cr^{VI} results in damage to the barrier layer.[34,42] Online measurements have shown that the transpassive dissolution of Ni-based alloys proceeds with elevated dissolution rates of Ni and Cr with the surface enrichment of Mo.[13] This process leads to increased currents which are slightly higher for the alloys with lower Cr contents. For all alloys, a secondary passive region was observed between ~0.4 V and 0.6 V. This was consistent with previous observations and attributed to surface enrichment with $Ni(OH)_2$.[43,44] For alloy G-30, this secondary passive region was extended to ~0.7 V (vs SCE), a feature attributed to the formation of insoluble Fe^{III} oxide.

In aerated 1 M HCl + 2 M NaCl solution, Fig. 7B, an active-to-passive transition was observed for all alloys except BC-1. The peak currents related to active dissolution were found to decrease with increasing Mo content as expected from published literature.[26,45] The observation of active behaviour for all alloys, except BC-1, was consistent with the E_{CORR}/R_P and EIS measurements, which indicated

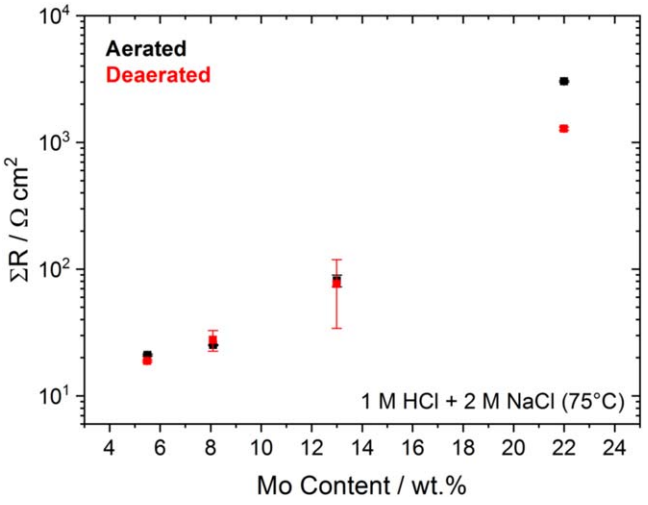

Figure 6. Relationship between Mo content and the total resistance (ΣR) calculated from equivalent circuit fitting of impedance spectra obtained in aerated and deaerated 1 M HCl + 2 M NaCl solution (75 °C). The error bars indicate the goodness of fit obtained from linear least squares fitting.

active behaviour for G-35, G-30 and C-22. For potentials more positive than the active-to-passive transition, where film formation occurred, the behaviour was complicated by a switch from anodic to cathodic current for alloys G-30 and G-35. For both alloys, the measured current eventually returned to anodic values as the applied potential was increased. Additionally, all alloys exhibited current transients, again with the exception of BC-1.

Polarization curves conducted in deaerated 1 M HCl + 2 M NaCl solutions, Fig. 7C, generally displayed higher currents through the passive region and yielded only anodic current values (∼−0.1 V to 0.8 V (vs SCE)), indicating that the net currents (j_{net}) in this potential region under aerated conditions were the sum of an anodic passive current (j_{anodic}) and a cathodic current ($j_{cathodic}$) for O_2 reduction. Consequently, the polarization curves acquired in deaerated solution allowed for j_{anodic} to be easily compared between alloys. For potentials immediately positive of the active-to-passive transition (i.e., up to ∼0.1 V (vs SCE)), the current was independent of potential for the three high Cr alloys and decreased as the Mo(W) content increased. At potentials ⩾0.1 V (vs SCE) the currents for the three alloys showed no consistent trend with composition, remained independent of potential for C-22 and G-30, and decreased with potential for G-35. The passive current for G-30, the high Fe containing alloy, was considerably higher than that of the other two alloys, indicating that the advantage of Fe in suppressing the current at high potentials in neutral solution was lost in acidic solutions, in which Fe^{3+} is much more soluble.[25] The current behaviour in this potential region (−0.1 V to 0.8 V) was significantly different to that of the other three alloys. While one to two orders of magnitude lower at the low end of this potential range, it increased steadily with potential to values approaching, and in the case of G-35 exceeding, the currents observed on alloys with lower Mo(W) contents.

The contributions from the cathodic current in the passive region were determined by subtracting the currents recorded in deaerated solution (j_{anodic}) from those measured in aerated solution ($j_{net} = j_{anodic} + j_{cathodic}$). The results are plotted against the applied potential for all four alloys in Fig. 8. Overall, no clear dependence of the current on the Mo(W)/Cr ratio was observed. For the alloy BC-1, with the highest Mo(W)/Cr ratio, the O_2 reduction current was effectively zero over the full potential range. For C-22 and G-35 relatively small values of $j_{cathodic}$ were observed, with the value for G-35 decreasing with increased potential while that for C-22 remained potential-independent. By far the largest cathodic current was observed for G-30, which differs significantly in composition from G-35 only in the Fe content. While transport processes were

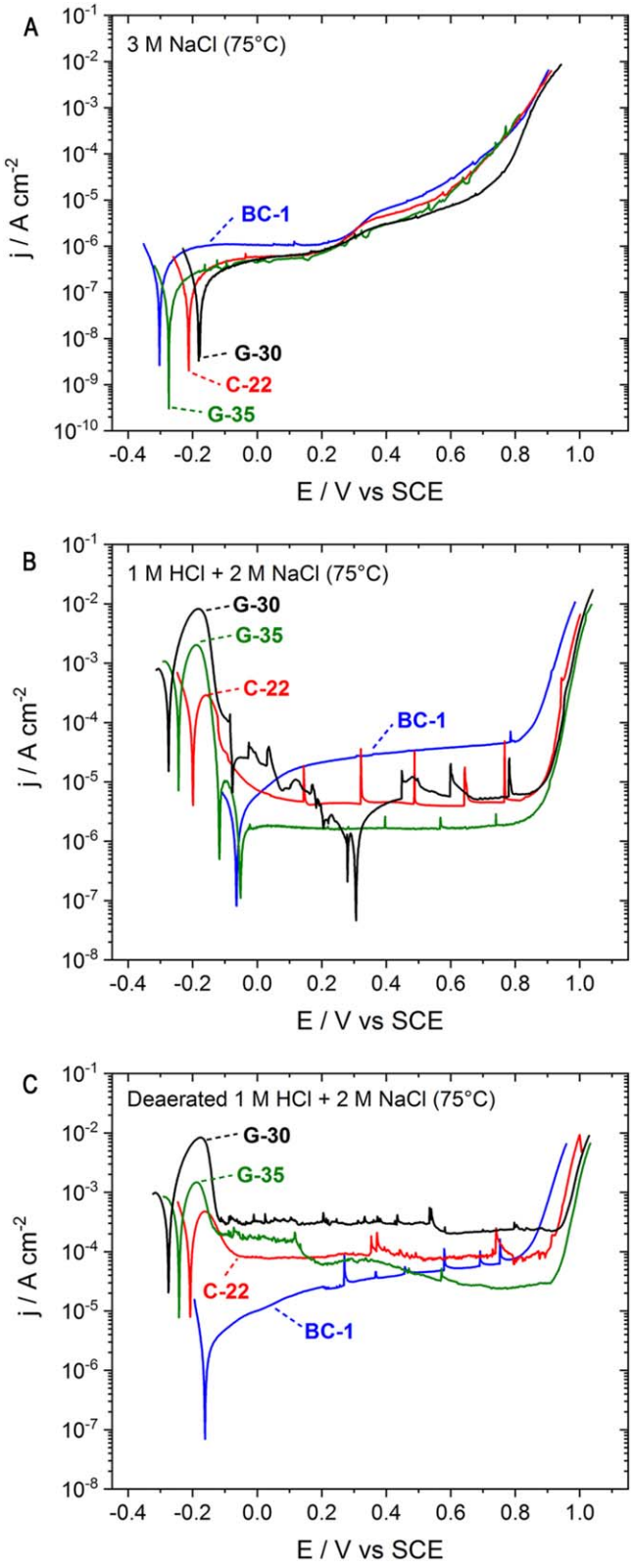

Figure 7. Polarization behaviour of alloys BC-1, C-22, G-35, and G-30 in (A) aerated 3 M NaCl, (B) aerated 1 M HCl + 2 M NaCl (B), and (C) deaerated 1 M HCl + 2 M NaCl (75 °C).

anticipated to limit the rate of O_2 reduction, especially at potentials far below the equilibrium potential, the large differences in cathodic currents for the alloys suggested presently unresolved chemical factors must also be involved.

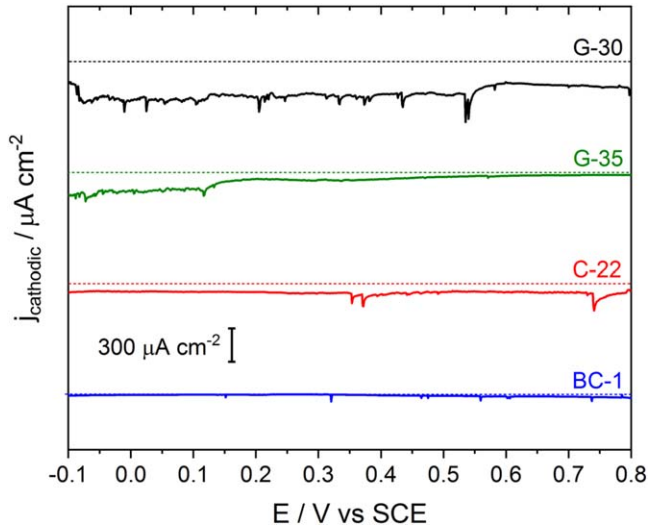

Figure 8. Cathodic current densities related to O_2 reduction throughout the region of film formation in 1 M HCl + 2 M NaCl (75 °C). Values obtained from the difference in current densities measured in naturally aerated and deaerated solutions; $j_{aerated} - j_{deaerated} = (j_{anodic} + j_{cathodic}) - j_{anodic}$. Dashed lines indicate the offset locations of $j = 0$.

In both aerated and deaerated acidic solutions, films formed at higher potentials were found to be susceptible to localized breakdown events. These instabilities were investigated in more detail under potentiostatic conditions. Figure 9A shows the currents recorded at an applied potential of 0 V (vs SCE) in deaerated 1 M HCl + 2 M NaCl. This potential was well above the active regions for those alloys which exhibited active behaviour but below potentials at which more unpredictable behaviour was observed, Fig. 7C. Figure 9B shows magnifications of individual transients for each alloy, which all exhibited the standard shape involving a rapid initiation followed by an exponential recovery. It is clear that the severity of breakdown and the time for recovery varies with the Mo (W) content of the alloy. However, the charge associated with individual transients was difficult to measure due to the long current tails for individual transients, in particular those recorded for the low Mo alloys, for which decay to the background passive current density was slow and incomplete.

The differences between the different alloys were characterized by determining the frequency of breakdown events and the maximum amplitude of individual events, Figs. 9C and 9D. The plotted values are based on 3–4 repeated experiments. This means the large error bars reflect an inability to totally capture the distributions of stochastic events. The frequency of breakdown events decreased markedly with increased alloy Mo(W) content, while the maximum current amplitude was low for all alloys except the high-Fe G-30 alloy. Interestingly, for this last alloy, the high frequency of high amplitude events led to a slow, but continuous, increase in the background passive current, indicating an inability of G-30 to completely repassivate.

Discussion

Passive films formed under neutral conditions.—In many studies, passive films grown at E_{CORR} have been characterized during or after exposure to acidic solution, where the release of the alloy matrix element, in this case Ni^{2+}, accelerates the enrichment of Cr and Mo within the oxide.[22,46] These films are commonly characterized by the enrichment of Cr at the alloy/oxide interface, while Mo segregates to the oxide/solution interface. However, a similar segregation process has also been demonstrated in air-formed oxide films,[33] indicating that it is a universal feature, irrespective of the oxidizing exposure environment. Consequently, such a process would be expected in our experiments in neutral solution.

The results in Fig. 3A indicate that the film resistance, R_f, while slightly lower for the Fe-containing G-30, is only marginally influenced by changes in Cr content ⩾22 wt.%. A significantly lower R_f was observed for alloy BC-1, containing the lowest Cr-content. At only ∼15 wt.%, the Cr content may be close to the minimum required to form the $–Cr^{III}–O^{II}–Cr^{III}–$ network necessary to establish a coherent Cr_2O_3 barrier layer. According to percolation theory, a critical cation fraction is required in the oxide to achieve a passive state in Fe- and Ni-based alloys containing Cr.[47,48]

Interestingly, a lower interfacial resistance, R_{int}, Fig. 3B, was observed for both BC-1 and C-22. As indicated in Fig. 3A, this was accompanied by a higher film capacitance, C_f, relative to the values measured for the two high-Cr alloys, G-30 and G-35. This combination of effects suggests that the inner layers present on BC-1 and C-22 are more defective than those on the other two alloys. Given the high Cr content of alloy C-22, it seems unlikely that the slightly inferior properties are attributable to a compositional inability to form a coherent $–Cr^{III}–O^{II}–Cr^{III}–$ network. A possibility is that the inner oxide found on BC-1 and C-22 has a higher Mo(W) content than that of the two high Cr alloys, caused by a more restricted segregation process in neutral solution where Ni^{2+} dissolution is limited. This would be consistent with recent studies that were interpreted based on the solute vacancy interaction model[49] and recent experiments indicating the likelihood that Mo is present in the form of individual cations, due to non-equilibrium solute capture in rapidly grown Ni^{II}/Cr^{III} oxides.[16]

It is possible that these lower values of R_{int} reflect a slower approach to a final steady-state passive film structure for these alloys. That this may be the case is suggested by the difference in relative values of R_P between the four alloys which are less divergent after 6 h of exposure than after shorter exposure times. For all four alloys, R_P values increase slightly over the full exposure period, suggesting a slow improvement in film properties, either due to thickening or to the elimination of point defects.

Passive films formed under acidic conditions.—The behaviour observed at E_{CORR} (Fig. 1) and under applied potential polarization (Fig. 7) confirms that, under acidic conditions, alloys G-35, G-30, and C-22 are active, while BC-1 maintains a weakly passive film, exhibiting passive current densities $>10^{-5}$ A cm^{-2}. In EIS experiments, the inductive response observed at low frequency, Fig. 4, is similar to behaviour commonly found on active metal surfaces, generally attributed to coupled electrochemical reactions involving adsorbed intermediates.[1,39] Inductive responses have been reported during the dissolution of Fe-based alloys in acid media[11,50–53] as well as for Ni,[54,55] Cr,[56,57] and Mo[58,59] systems. Since all of these elements are found in the studied alloys, inductive responses are to be expected. It is likely that the oxidation of each of these metal cations involves adsorbed states, some possibly involving the co-adsorption of anions as well.

Both Jakupi et al.[60] and Ebrahimi et al.[4] showed that Mo was retained at active sites under the active corrosion conditions prevailing inside a propagating crevice, while Ni and Cr were not. More recently, Li and Ogle confirmed[46] that similar behaviour, involving only the retention of Mo, was observed under active conditions not involving a crevice geometry. Jakupi et al.[60] investigated the nature of Mo deposits formed inside an actively corroded crevice using Raman spectroscopy. While they found it difficult to be specific, due to the complexity of the Mo polymerization process, this study indicated the presence of MoO_2, Mo_4O_{11} and ill-defined polymeric species such as $Mo_{36}O_{112}^{8-}$. When W was present, no spectral differences were observed, although W would be expected to exert a similar response to Mo. Bojinov et al.[58] proposed a complex anodic reaction sequence for Mo involving multiple adsorbed species with an initial step in which Mo^{III} was reversibly converted to Mo^{IV}.

The change in behaviour from active, involving inductive responses in the EIS, to passive, involving a capacitive response, as the Mo(W) content of the alloy increased could then possibly be explained by a shift from reversible adsorbed states at low Mo contents to the MoO_2

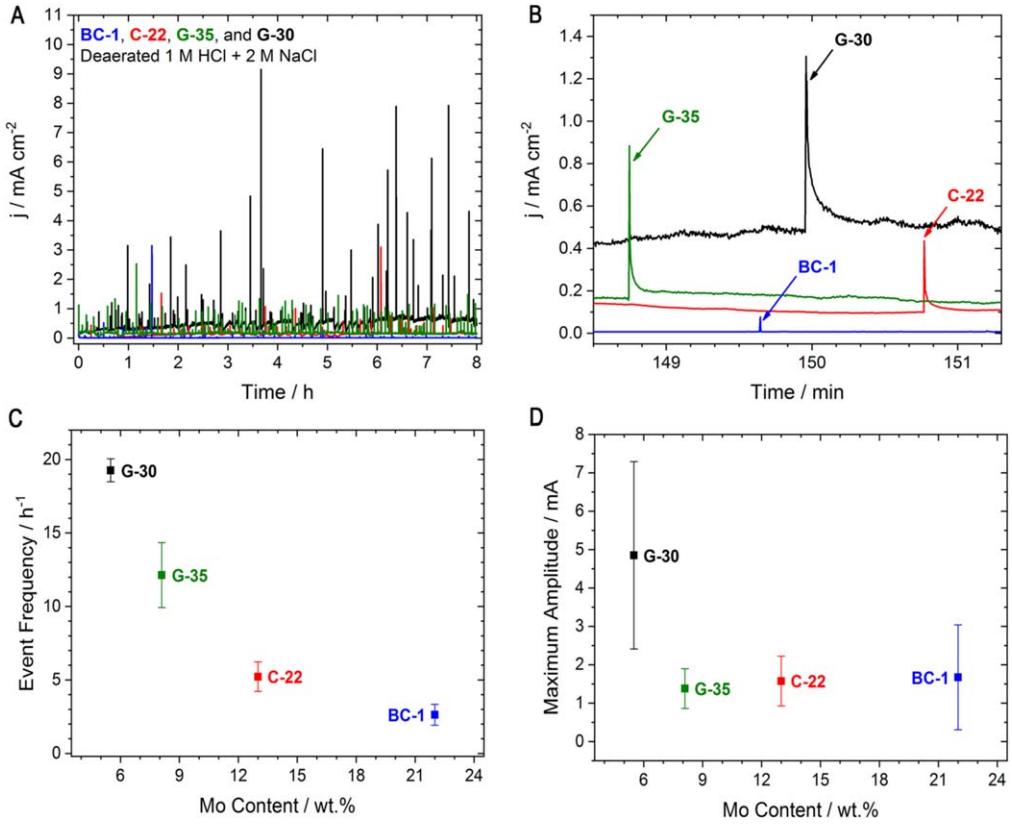

Figure 9. Current-time response of potentiostatic experiments at 0 V (vs SCE) on alloys BC-1, C-22, G-35, and G-30 in deaerated 1 M HCl + 2 M NaCl (75 °C). Data collected over an 8 h period are shown in (A), while (B) shows a magnified region for better comparison of current transients. Quantification of the average event frequency and maximum amplitude is given in (C) and (D), respectively.

and polymeric species at higher contents. The observation of an active-passive transition for G-30, G-35 and C-22 confirms the occurrence of active behaviour, with the absence of such a transition for BC-1 expected in the presence of a corrosion-resistant Mo oxide/molybdate layer. At low potentials in the passive region (as defined by the polarization curves in the absence of O_2, Fig. 7C) the lower passive current in higher-Mo(W) alloys demonstrates that the Mo(W) content is crucial in sustaining passivity and in suppressing the events which initiate localized film breakdown.[14,20–26,29,61–63]

The ability of Mo to enhance the passivity of Fe-based alloys has been explained in terms of a bipolar model[29] with an outer layer Mo-oxide protecting an inner Cr^{III} barrier layer. It was proposed that the outer layer contained anionic Mo species (e.g. MoO_4^{2-}), giving the oxide/solution interface a certain cation selective nature to repel aggressive anions, such as Cl^-, which would induce film breakdown. As noted by Lutton Cwalia et al.[12] this segregation process facilitates the formation of a continuous Cr_2O_3 layer and suppresses cation vacancy motion. Thus, while this model offers an explanation for a decrease in the number of attempted breakdown events as the Mo (W) content increases, it does not necessarily explain the suppression of the current amplitude when transients do occur. As shown in Fig. 9, as the Mo(W) content decreases, transients become more frequent and severe compared to those on high-Mo alloys. It is well-established that Mo-rich corrosion products deposit in areas of active corrosion and supress active behaviour.[4,10,19] Recent studies by Li and Ogle[46] show that when the potential applied to C-22 is in an active region (in 2 M H_2SO_4), Ni, Cr, and Fe are released to solution, but not Mo. This indicates that a breakdown event in a passive oxide would retain Mo(W) at the breakdown site at a rate dictated by the Mo(W) content of the alloy. This is consistent with the observations of Maurice et al.[14] who observed the accumulation of Mo at nanoscale defects in the passive film formed on an Fe-based single crystal containing Cr, Ni, and Mo additions.

The role of the oxygen reduction reaction.—While H^+ reduction is the dominant cathodic reaction observed in polarization curves recorded in aerated acidic solution, O_2 reduction also occurs throughout the passive region, Fig. 8. Previously, Zhang et al.[38] explored the kinetics of the O_2 reduction (in neutral 5 M NaCl at 70 °C) in relation to oxide film properties on alloy C-22. They found that higher rates of O_2 reduction occurred on films which had been damaged and subsequently repaired. They attributed the increased rate to either enriched Mo-species, which could catalyze the reaction, or a more defective oxide film structure. It was later shown that Mo enrichment during film breakdown is a dynamic process, meaning that Mo-species quickly accumulate, then are subsequently removed during film repair.[13] As a result, the observations made by Zhang et al., as well as those in this study, indicate that it is the presence of oxide defects that leads to increased cathodic activity. Since O_2 reduction currents show little dependence on potential, Fig. 8, and were proportional to the passive current densities (Fig. 7C), it appears that the rate of O_2 reduction was dependent on the physical properties of the passive film (possibly defect structure and composition) with a possible influence of transport for alloy G-30.

Conclusions

The relationship between Cr and Mo alloying additions was investigated during the corrosion of commercially available Ni-based alloys in both neutral and acidic chloride solutions. In neutral solution, corrosion rates were found to be dependent on the Cr content at both E_{CORR} and other applied potentials. All alloys appeared to be immune to localized corrosion in neutral chloride solutions in these experiments, likely a result of the sufficiently high Mo content (⩾5.5 wt.% Mo). In contrast to those made in the neutral solution, electrochemical measurements made in acidic chloride

solution suggest that Mo becomes increasingly important to the alloy's corrosion performance and provides two distinct benefits.

Firstly, alloyed Mo was found to increase the stability of the passive film during exposure to acidic solution. During corrosion at E_{CORR}, the alloy with the highest Mo content, BC-1 (22 wt.% Mo), was found to retain a partially protective oxide film even in 1 M HCl + 2 M NaCl solution. This resulted in polarization resistance values that were approximately two orders of magnitude higher than those recorded for the alloys with lower Mo contents; C-22, G-35, and G-30. Furthermore, the impedance spectra collected on low-Mo alloys demonstrated low-frequency inductive features, consistent with a dissolution mechanism involving adsorbed intermediates. During potentiodynamic experiments, increased Mo content was found to suppress features of active dissolution and, unexpectedly, alloys G-35 and G-30 displayed a transition from net anodic to net cathodic current at applied potentials higher than the active-passive transition. The removal of O_2, the anticipated cathodic reagent, allowed us to show that, while Cr appears to dictate the properties of this film in aerated solutions, in fact it is Mo that stabilizes the film. Secondly, a higher Mo content was found to benefit the repassivation behaviour of alloys exposed to acidic chloride solution. Localized events on oxides grown at fixed potentials occur with a higher frequency and severity on low-Mo alloys.

Here, a summary of the relationship between Cr/Mo additions in commercially relevant alloys has been given. Findings suggest that a balance should be maintained between additions of Cr and Mo, although the optimal composition remains unknown. Indeed, the transient and pH-dependent nature of the Mo oxide response to corrosive conditions suggest that the optimal Cr/Mo(W) ratio may differ by exposure environment. Since localized corrosion is of concern in most applications that expose the alloy to chloride, the Mo content should be strongly considered during alloy selection for its ability to both stabilize the oxide film and repair localized breakdown sites.

Acknowledgments

Haynes International is acknowledged for supplying the Hastelloy alloys used in this study. Author J.D.H. would like to thank B.A. and S.A. for their hard work during their fourth-year undergraduate research projects and contributions to this study. Author J.D.H. is grateful to be the recipient of an Alexander Graham Bell Canada Graduate Scholarship (NSERC), the 2018 H.H. Uhlig Summer Fellowship (ECS), and the 2019 Canada section Student Award (ECS).

ORCID

Jeffrey D. Henderson https://orcid.org/0000-0001-7415-756X
Vahid Dehnavi https://orcid.org/0000-0002-8429-002X

References

1. P. Marcus, *Corrosion Mechanisms in Theory and Practice* (CRC press, Boca Raton, FL) (2011).
2. N. Priyantha, P. Jayaweera, D. D. Macdonald, and A. Sun, *J. Electroanal. Chem.*, **572**, 409 (2004).
3. N. Dong, C. Zhang, H. Li, B. Zhang, and P. Han, *Sci. Rep.*, **7**, 1 (2018).
4. N. Ebrahimi, P. Jakupi, J. J. Noël, and D. W. Shoesmith, *Corrosion*, **71**, 1441 (2015).
5. M. Pourbaix, *Atlas of Electrochemical Equilibria in Aqueous Solution* (NACE, Houston, TX) (1974).
6. A. K. Mishra and D. W. Shoesmith, *Corros. Sci.*, **70**, 721 (2014).
7. N. Sridhar, J. B. C. Wu, and P. E. Manning, *JOM*, **37**, 51 (1985).
8. R. B. Rebak and J. H. Payer, *Passive Corrosion Behaviour of Alloy 22*, U.S. Department of Energy Office of Scientific and Technical Information (2006).
9. M. B. Rockel, *Corrosion*, **29**, 393 (1973).
10. X. Shan and J. H. Payer, *Journal of The Electochemical Society*, **156**, C313 (2009).
11. M. Bojinov, I. Betova, and R. Raicheff, *J. Electroanal. Chem.*, **430**, 169 (1997).
12. K. Lutton Cwalina, C. R. Demarest, A. Y. Gerard, and J. R. Scully, *Current Opinions in Solid State & Materials Science*, **23**, 129 (2019).
13. J. D. Henderson, X. Li, D. W. Shoesmith, J. J. Noël, and K. Ogle, *Corros. Sci.*, **147**, 32 (2019).
14. V. Maurice, H. Peng, L. H. Klein, A. Seyeux, S. Zanna, and P. Marcus, *Faraday Discuss.*, **180**, 151 (2015).
15. C. D. Taylor, P. Lu, J. Saal, G. S. Frankel, and J. R. Scully, *Npj Materials Degradation*, **2**, 1 (2018).
16. X. X. Yu, A. Gulec, C. M. Andolina, E. J. Zeitchick, K. Gusieva, J. C. Yang, J. R. Scully, J. H. Perepezko, and L. D. Marks, *Corrosion*, **74**, 939 (2018).
17. J. W. Oldfield and W. H. Sutton, *Br. Corros. J.*, **13**, 104 (1978).
18. M. Nishimoto, J. Ogawa, I. Muto, Y. Sugawara, and N. Hara, *Corros. Sci.*, **106**, 298 (2016).
19. N. Ebrahimi, J. J. Noël, M. A. Rodriguez, and D. W. Shoesmith, *Corros. Sci.*, **105**, 58 (2016).
20. J. D. Henderson, N. Ebrahimi, V. Dehnavi, M. Guo, D. W. Shoesmith, and J. J. Noël, *Electrochim. Acta*, **283**, 1600 (2018).
21. H. Huang, *Biomaterials*, **24**, 1575 (2003).
22. A. C. Lloyd, J. J. Noël, N. S. McIntyre, and D. W. Shoesmith, *J. Met.*, **57**, 31 (2005).
23. A. C. Lloyd, J. J. Noël, S. McIntyre, and D. W. Shoesmith, *Electrochim. Acta*, **49**, 3015 (2004).
24. Y. Dou, S. Han, L. Wang, X. Wang, and Z. Cui, *Corros. Sci.*, **165**, 108405 (2020).
25. C. F. Baes and R. E. Mesmer, *The Hydrolysis of Cations* (Wiley, New York) (1976).
26. A. Mishra, D. W. Shoesmith, and P. Manning, *Corrosion*, **73**, 68 (2017).
27. R. Newman, *Corros. Sci.*, **25**, 341 (1985).
28. R. Newman, *Corros. Sci.*, **25**, 331 (1985).
29. C. R. Clayton and Y. C. Lu, *Journal of The Electochemical Society*, **133**, 2465 (1986).
30. E. Gardin, S. Zanna, A. Seyeux, A. Allion-Maurer, and P. Marcus, *Corros. Sci.*, **143**, 403 (2018).
31. X. Zhang and D. W. Shoesmith, *Corros. Sci.*, **76**, 424 (2013).
32. X. Zhang, D. Zagidulin, and D. W. Shoesmith, *Electrochim. Acta*, **89**, 814 (2013).
33. J. D. Henderson, A. Seyeux, S. Zanna, M. C. Biesinger, D. W. Shoesmith, J. J. Noël, and P. Marcus, *Corros. Sci.*, **159**, 108138 (2019).
34. P. Jakupi, D. Zagidulin, J. J. Noël, and D. W. Shoesmith, *Electrochim. Acta*, **56**, 6251 (2011).
35. N. Ebrahimi, M. C. Beiesinger, D. W. Shoesmith, and J. J. Noël, *Surface Interface Analysis*, **49**, 1359 (2017).
36. K. Lutton, K. Gusieva, N. Ott, N. Birbilis, and J. R. Scully, *Electrochem. Commun.*, **80**, 44 (2017).
37. J. J. Gray and C. A. Orme, *Electrochim. Acta*, **52**, 2370 (2007).
38. X. Zhang, Z. Qin, D. Zagidulin, J. J. Noël, and D. W. Shoesmith, *Journal of The Electochemical Society*, **164**, C911 (2017).
39. M. E. Orazem and B. Tribollet, *Electrochemical Impedance Spectroscopy* (Wiley, New York) (2017).
40. B. Hirschorn, M. E. Orazem, B. Tribollet, V. Vivier, I. Frateur, and M. Musiani, *Electrochim. Acta*, **55**, 6218 (2010).
41. G. J. Brug, A. L. G. van den Eeden, M. Sluyters-Rehbach, and J. H. Sluyters, *J. Electroanal. Chem. Interfacial Electrochem.*, **176**, 275 (1984).
42. M. Bojinov, G. Fabricius, T. Laitinen, T. Saario, and G. Sundholm, *Electrochim. Acta*, **44**, 247 (1998).
43. A. K. Mishra and D. W. Shoesmith, *Electrochim. Acta*, **102**, 328 (2013).
44. A. K. Mishra, S. Ramamurthy, M. Biesinger, and D. W. Shoesmith, *Electrochim. Acta*, **100**, 118 (2013).
45. E. McCafferty, *Introduction to Corrosion Science* (Springer, Berlin New York) (2010).
46. X. Li and K. Ogle, *J. Electrochem. Soc.*, **166**, C3179 (2019).
47. E. McCafferty, *J. Electrochem. Soc.*, **155**, C501 (2008).
48. E. McCafferty, *Corros. Sci.*, **50**, 3622 (2008).
49. M. Urquidi and D. D. Macdonald, *Journal of The Electochemical Society*, **132**, 555 (1985).
50. D. C. Silverman, *Electrochim. Acta*, **38**, 2075 (1993).
51. A. Pardo, M. C. Merino, A. E. Coy, F. Viejo, R. Arrabal, and E. Matykina, *Corros. Sci.*, **50**, 780 (2008).
52. G. Bellanger and J. J. Rameau, *J. Nucl. Mater.*, **228**, 24 (1996).
53. S. Naharajan and N. Rajendran, *Corros. Sci.*, **51**, 217 (2009).
54. G. Cordeiro and O. R. Mattos, *J. Appl. Electrochem.*, **26**, 1083 (1996).
55. M. R. Barbosa, J. A. Bastos, J. J. Garcia-Jareno, and F. Vicente, *Electrochim. Acta*, **44**, 957 (1998).
56. J. A. L. Dobbelaar and J. H. W. de Wit, *Journal of The Electochemical Society*, **137**, 2038 (1990).
57. A. I. Karayan, E. Maya-Visuet, and H. Castaneda, *J. Solid State Electrochem.*, **18**, 3191 (2014).
58. M. Bojinov, I. Betova, and R. Raicheff, *Electrochim. Acta*, **41**, 1173 (1996).
59. R. D. Armstrong, M. F. Bell, and A. A. Metcalfe, *J. Electroanal. Chem.*, **84**, 61 (1977).
60. P. Jakupi, F. Wang, J. J. Noël, and D. W. Shoesmith, *Corros. Sci.*, **53**, 1670 (2011).
61. G. Frankel et al., *Faraday Discuss.*, **180**, 381 (2015).
62. J. R. Scully, *Faraday Discuss.*, **180**, 577 (2015).
63. D. D. Macdonald, *Russ. J. Electrochem.*, **48**, 235 (2012).